Molecular basis for complement recognition by integrin $\alpha_X\beta_2$

Xing Chen[a,1], Yamei Yu[a], Li-Zhi Mi[a], Thomas Walz[b], and Timothy A. Springer[a,2]

[a]Immune Disease Institute, Children's Hospital Boston, and Department of Biological Chemistry and Molecular Pharmacology, Harvard Medical School, Boston, MA 02115; and [b]Howard Hughes Medical Institute and Department of Cell Biology, Harvard Medical School, Boston, MA 02115

Contributed by Timothy A. Springer, February 6, 2012 (sent for review November 9, 2011)

Integrin $\alpha_X\beta_2$ functions as complement receptor for iC3b and mediates recognition and phagocytosis of pathogens. We used negative-stain EM to examine the $\alpha_X\beta_2$ interaction with iC3b. EM class averages of $\alpha_X\beta_2$ in complex with iC3b define the binding sites on both the integrin and iC3b. iC3b contains C3c and thioester domain moieties linked by a long flexible linker. The binding site is on the key ring of the C3c moiety, at the interface between the MG3 and MG4 domains. Similar complexes are seen between $\alpha_X\beta_2$ and the C3c fragment. $\alpha_X\beta_2$ binds through the α_X αI domain, on the face known to bear the metal ion-dependent adhesion site, at the opposite end of the αI domain from its site of insertion in the β-propeller domain.

The human complement system is an essential component of host defense and plays an important role in linking innate and adaptive immunity (1, 2). The third complement component, C3, and its activation products are pivotal both in amplification of the complement pathway and in opsonization of foreign particles for immune recognition and phagocytosis. C3 is proteolytically activated to C3b, which covalently attaches through the thioester domain (TED) to immune complexes and pathogen surfaces (Fig. 1*A*). Sequential cleavages convert C3b to iC3b, and then to its terminal fragment C3dg, which remains covalently attached through TED, and C3c, which is released into the fluid phase. Five different complement receptors (CRs) show specificity for distinct C3 fragments. X-ray structures of C3, C3b, and C3c, as well as the CR receptor CRIg in complex with C3b and C3c, have shed light on the regulation of complement activation (3–5). EM structures of C3 and its activation products not only confirmed these crystal structures but yielded information on the activation intermediate C3(N)*, similar to C3b* (6), and iC3b (6, 7) (Fig. 1*A*). iC3b was found to consist of two moieties. A key ring-like C3c subregion and a thioester–bond-containing domain (TED) are connected by an ∼50-Å long flexible region corresponding to the portion of the CUB domain that remains after factor I cleavage (6). Another group reported some data consistent with the above structure (*Discussion*), as well as other results supporting a specific interaction in iC3b between the C3c region and the CUB and TED domains (7).

CR types 3 and 4 (CR3 and CR4) were originally defined functionally by their selectivity for rosetting with iC3b-sensitized erythrocytes compared with C3b and C3d, and unique cell distribution compared with CR1 and CR2 (8). CR3 and CR4 are of great importance for recognition and phagocytosis of pathogens and immune complexes in vivo (9) and in pathogenesis of disease, including acute glomerulonephritis (10). Subsequently, CR3 function was found to be selectively inhibited by antibodies specific for the integrin Mac-1 ($\alpha_M\beta_2$, CD11b/CD18) (11). Furthermore, both CR3 and CR4 (integrin $\alpha_X\beta_2$, CD11c/CD18) were specifically isolated from cells by affinity chromatography on iC3b-Sepharose (12). CR4 has the same specificity as CR3, although stronger cellular activation is required to activate CR4 (13). Purified CR4 and CR4 transfectants specifically bind iC3b-opsonized erythrocytes (14).

$\alpha_M\beta_2$ and $\alpha_X\beta_2$ are closely related with 60% amino acid sequence identity in their α-subunits and identical β-subunits, and they recognize a bewildering and largely overlapping array of ligands, including denatured proteins (15, 16). iC3b is the first identified and perhaps the most specifically recognized of these ligands. Surface plasmon resonance studies have shown higher affinity of a mutant, high-affinity α_X I domain for iC3b than for other ligands, such as fibrinogen (17, 18). However, the molecular basis for selectivity of $\alpha_X\beta_2$ for iC3b in rosetting assays and the binding site within iC3b have not been defined. Initially, the closely related integrin $\alpha_M\beta_2$ (CR3) was reported to bind to an Arg-Gly-Asp (RGD) sequence within iC3b based on inhibition with peptides (19). However, subsequent mutagenesis of the RGD site showed no effect on $\alpha_M\beta_2$ binding (20). Further study suggested involvement of an acidic region at the N terminus of the α′-chain of C3 in binding to both CR1 and CR3 (21). Antibodies to the αI domain of CR4 inhibited binding to iC3b, suggesting participation of the αI domain in ligand binding (14). A large number of mutational and antibody blocking studies have also demonstrated the critical role of the αI domain of the integrin αM subunit in CR3 function (22–25). However, the αM subunit β-propeller domain and β2 subunit βI domain of CR3 have also been implicated in iC3b binding (26–28).

Here, we report negative-stain EM studies of $\alpha_X\beta_2$ in complex with complement components iC3b and C3c. The results show that the binding site is within the C3c fragment, near the junction of MG3 and MG4 domains.

Results

In this study, we used exactly the same ectodomain preparation that was used to determine the crystal structure of $\alpha_X\beta_2$ (29). This construct appends to the C termini of the α- and β-subunits a GCG sequence with a cysteine residue that forms an intersubunit disulfide bond, a 12-residue linker containing a tobacco etch virus (TEV) protease site, ACID/BASE coiled coils, and purification tags (Fig. 1*B*). After purification, the coiled coils were removed by TEV protease digestion. Negative-stain EM shows that this construct adopts both the bent and extended-closed headpiece conformations, at about a 1:1 ratio (29), and converts to the extended-open headpiece conformation in the presence of the activating Fabs CBR LFA-1/2 and KIM127 (Fig. S1). This behavior differs from that of a construct lacking a GCG sequence and containing coiled coils, which is basally almost completely bent, and adopts both the extended-closed headpiece and the extended-open headpiece conformations in the presence of CBR LFA-1/2 and KIM127 Fabs (30, 31).

On cell surfaces, integrins must be activated to bind ligands with high affinity. We tested different combinations of Fab and Mn^{2+} for activating binding of $\alpha_X\beta_2$ to iC3b. The best condition we found for isolation of $\alpha_X\beta_2$–iC3b complexes stable to gel

Author contributions: T.A.S. designed research; X.C. and Y.Y. performed research; Y.Y. contributed new reagents/analytic tools; X.C., L.-Z.M., T.W., and T.A.S. analyzed data; and X.C., T.W., and T.A.S. wrote the paper.

The authors declare no conflict of interest.

[1]Present address: College of Chemistry and Molecular Engineering, Peking University, Beijing 100871, People's Republic of China.

[2]To whom correspondence should be addressed. E-mail: springer@idi.harvard.edu.

This article contains supporting information online at www.pnas.org/lookup/suppl/doi:10.1073/pnas.1202051109/-/DCSupplemental.

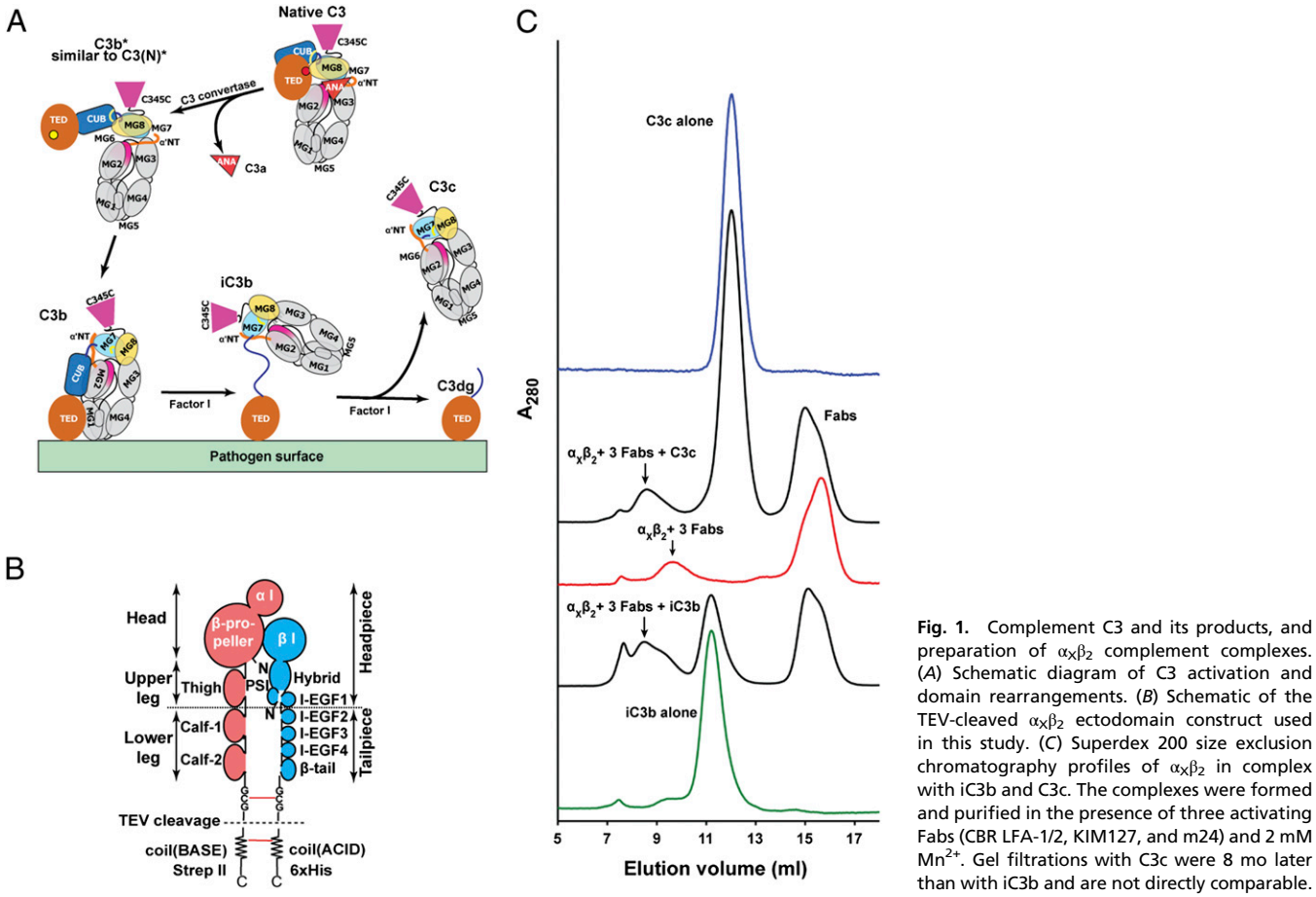

Fig. 1. Complement C3 and its products, and preparation of $\alpha_X\beta_2$ complement complexes. (*A*) Schematic diagram of C3 activation and domain rearrangements. (*B*) Schematic of the TEV-cleaved $\alpha_X\beta_2$ ectodomain construct used in this study. (*C*) Superdex 200 size exclusion chromatography profiles of $\alpha_X\beta_2$ in complex with iC3b and C3c. The complexes were formed and purified in the presence of three activating Fabs (CBR LFA-1/2, KIM127, and m24) and 2 mM Mn^{2+}. Gel filtrations with C3c were 8 mo later than with iC3b and are not directly comparable.

filtration was with three activating Fabs (CBR LFA-1/2, KIM127, and m24) and inclusion of 2 mM Mn^{2+} in all buffers. The $\alpha_X\beta_2$ complex with three Fabs and iC3b eluted earlier than the $\alpha_X\beta_2$ complex with three Fabs only (Fig. 1*C*). CBR LFA-1/2 and KIM127 induce integrin extension, whereas m24 stabilizes the open integrin headpiece, which has high affinity for ligand (31). Use of only the two extension-inducing antibodies, CBR LFA-1/2 and KIM127, with 2 mM Mn^{2+} gave only partial complex formation in gel filtration, and did not yield sufficient complexes on grids for EM analysis.

Some class averages showed clear density for both the C3c moiety of iC3b and $\alpha_X\beta_2$ (Fig. 2*A* and Fig. S2). In many class

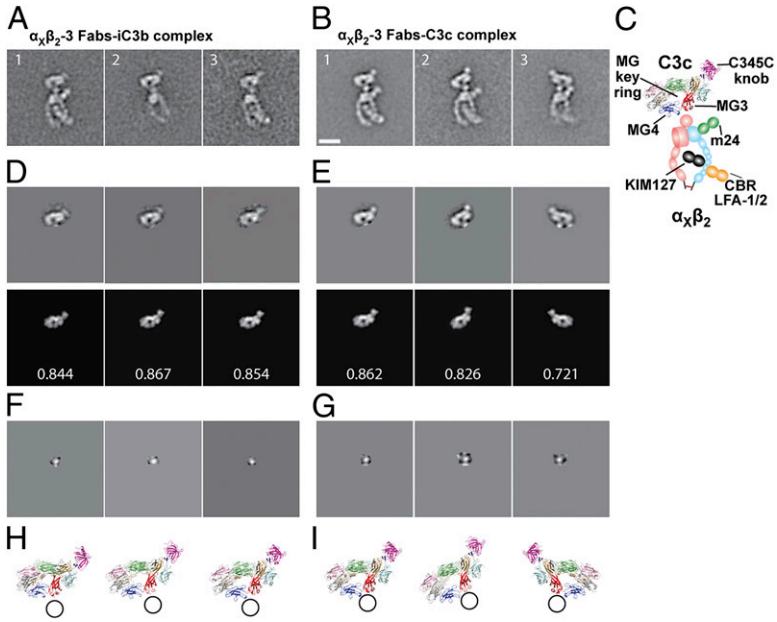

Fig. 2. Negative-stain EM of $\alpha_X\beta_2$ complement complexes and cross-correlation between EM class averages and crystal structure projections. Better resolved class averages of complexes of $\alpha_X\beta_2$ and Fabs of CBR LFA-1/2, KIM127, and m24 in 2 mM Mn^{2+} with iC3b (*A*) and C3c (*B*). (Scale bars, 10 nm.) (*C*) Schematic interpretation of averages in *A* and *B*. The binding sites for each of the three Fabs have previously been determined (31). (*D* and *E*) Mask for the C3c moiety (*Upper*) and best correlating C3c crystal structure projection (5) (*Lower*) for the class averages shown above. (*F* and *G*) Mask for the α_X αI domain moiety. (*H* and *I*) Ribbon diagrams of C3c and a circle representing the position of the α_X αI domain, in exactly the same orientation and spatial relationship as established by cross-correlation using the masks shown above and enlarged.

averages, however, the density of either iC3b or $\alpha_X\beta_2$ was smeared out, suggesting that the interaction surface between the two molecules is small, resulting in different relative orientations. In class averages in which all three Fabs were resolved, they bound to the same integrin domains as previously described: m24 to the βI domain, KIM127 to the I-EGF2 domain, and CBR LFA-1/2 to the I-EGF3 domain (31) [Fig. 2*A* (panel 1) and *C*]. $\alpha_X\beta_2$ adopted the extended-open headpiece conformation (Fig. 2*A*). These results are consistent with the finding that this is the conformation that has high affinity for ligand and that m24 Fab selectively binds to and stabilizes the open headpiece conformation (31).

The binding site between iC3b and $\alpha_X\beta_2$ was clearly defined and the same in all well-resolved class averages. $\alpha_X\beta_2$ bound only to iC3b through its αI domain, on the face of the αI domain opposite to the α_X β-propeller and β_2 βI domains (Fig. 2*A*). This iC3b-binding face is that known from crystal structures to bear the metal ion-dependent adhesion site (MIDAS) (29). iC3b bound only through its C3c moiety, on the key ring formed by its MG domains (Fig. 2 *A* and *C*).

The TED moiety of iC3b did not interact with $\alpha_X\beta_2$, and did not appear in class averages. This is consistent with the previous observation that the linkage between the C3c and TED moieties in iC3b is flexible, and that the TED moiety frequently was "averaged out" and not seen in iC3b class averages (6). The integrin and the three Fabs are much greater in mass than the TED, and thus are expected to dominate in class averaging (*Discussion*). The markedly earlier elution of the iC3b than C3c in gel filtration confirmed the presence of the TED. To confirm this further, we used the same EM grids from the iC3b–integrin–Fab complex peak in gel filtration, and picked particles from which the integrin had dissociated (Fig. S2*C*). Class averages showed that the TED domain was visible in some class averages, and was randomly oriented with respect to the C3c moiety (Fig. 3) whereas the TED domain was not resolved in other class averages (Fig. S2*D*), exactly as reported previously (6).

Based on these observations, we predicted that C3c should also bind to $\alpha_X\beta_2$. Indeed, C3c complexed with $\alpha_X\beta_2$ in the presence of three Fabs and Mn^{2+}, as shown by elution position in gel filtration (Fig. 1*C*). EM of the complex peak revealed that the β-propeller distal face of the α_X I domain bound to the key ring of C3c (Fig. 2*B* and Fig. S3), with a complex structure identical to that seen in iC3b (Fig. 2 *A* and *B*). In some class averages, C3c flipped 180° with respect to $\alpha_X\beta_2$ but maintained the same site of interaction on the key ring with the α_X I domain (Fig. 2*B*, panel 6). We attribute flipping to the tendency of proteins to lie flat on EM substrates. The C3c moiety of iC3b, C3c, and the $\alpha_X\beta_2$–Fab complex each oriented on the EM substrate through relatively planar faces that have large contact areas for the substrate. We interpret the results as suggesting that when free in solution, the $\alpha_X\beta_2$ headpiece and C3c moiety are not as coplanar as they appear in 2D images, and that the orientation between their planes when not constrained by adsorption to a planar surface is closer to the predominant than the minority orientation seen in class averages. We also note that the α_X I domain is flexible with respect to the α_X β-propeller and βI domains (29).

Visual inspection showed that the α_X I domain bound to the least dense portion of the MG key ring at MG3 and MG4 domains, where the ring is only one MG domain thick (Fig. 1*A* and Fig. 2 *A*–*C*). This location was also verified by the direction of the cock formed by the C345c knob (Fig. 2*C*). The binding site was further pinpointed by cross-correlation. All but the C3c moiety was masked from averages of integrin complexes with iC3b or C3c (Fig. 2 *D* and *E*, *Upper*). These showed excellent cross-correlation with the C3c crystal structure (Fig. 2 *D* and *E*, *Lower*). The projections with the highest cross-correlation coefficients correspond to the orientation of the ribbon diagrams of C3c (Fig. 2 *H* and *I*), which are also in excellent agreement with the corresponding class averages in Fig. 2 *A* and *B*. The position of the α_X I domain was further determined by cross-correlation to appropriately masked class averages (Fig. 2 *F* and *G*), and is shown as a circle in Fig. 2 *H* and *I*. The cross-correlations establish that the binding site in the C3c moiety locates to the interface between the MG3 and MG4 domains, which is decorated by multiple loops from both MG3 and MG4.

Discussion

Here, we visualize by EM how integrin $\alpha_X\beta_2$ binds to its physiological ligand, complement component iC3b. Our results define the domains in both the integrin and iC3b that mediate the interaction. In this study, binding of a complete αI-integrin ectodomain to a ligand has been structurally characterized. Previous studies with isolated αI domains have shown how a binding site centered on the αI MIDAS binds the residues in collagen triple helical fragments (α_2 I domain) (32) or in intercellular adhesion molecules (α_L I domain) (33, 34). Our results confirm the conclusion that the αI domain is the primary ligand-binding site in αI integrins (16, 35). More specifically, we show that the α_X I domain in CR4 is the binding site for iC3b and confirm previous findings that antibodies to the αI domain specifically inhibit binding to iC3b by intact CR4 (14) and that an isolated, high-affinity mutant αI domain binds to iC3b with a K_d of 2.4 μM (17).

Integrins assume three overall conformational states on cell surfaces, and effector molecules that bind to integrin cytoplasmic domains regulate the equilibrium between these conformational states, and hence affinity for ligand (36). Studies with integrin $\alpha_X\beta_2$ have shown that the bent integrin (which has a closed headpiece) and the extended integrin with a closed headpiece each have low affinity for ligand. Only the extended integrin with an open headpiece has high affinity for ligand (31). Agents that only partially shift the equilibrium, such as extension-promoting Fabs or Mn^{2+}, are sufficient to induce binding of cell-surface integrins or substrate-bound purified $\alpha_X\beta_2$ to erythrocytes sensitized with iC3b (31). The more stringent requirements found here for formation of soluble $\alpha_X\beta_2$ complexes with iC3b, including the use of a Fab that stabilizes the open integrin headpiece, are to be expected for the monovalent interaction studied here, which contrasts with previous studies of multivalent interactions with cells sensitized with iC3b.

The CR4 α_X subunit and CR3 α_M subunit are 60% identical in amino acid sequence, and their β_2 subunits are identical; therefore, CR3 and CR4 are expected to bind similarly to iC3b. Similar to CR4, most previous studies on CR3 have found that the αI domain binds to iC3b (22–25). However, other studies have identified additional contributions to iC3b binding by the β-propeller and β_2 I domains of CR3 (26–28). These studies were carried out before crystal structures of CR4 were elucidated (29) and before demonstration of the importance of headpiece opening in integrin affinity regulation (36), and it is now appropriate to interpret them in light of these developments. By way of introduction, both integrin α- and β-subunits contain I domains, known as αI and βI domains, respectively. Both contain a MIDAS, with a DXSXS motif that binds Mg^{2+}. The βI domain regulates ligand binding by the αI domain by a mechanism in which the βI domain MIDAS binds a Glu residue that follows the αI domain C-terminal α-helix and relays activation to the αI domain MIDAS. The integrin α-subunit β-propeller domain and the β-subunit βI domain form a pocket that binds this Glu residue and surrounding conserved hydrophobic residues (29). Thus, mutations of residues in the DXSXS motif of the βI domain inhibit ligand binding to the αI domain (37). The formation of an active binding pocket at the βI domain MIDAS, in turn, requires relay of allostery from the βI domain interface with the hybrid domain. The marked change in βI-hybrid domain orientation at this interface has been characterized by crystal structures, and can be distinguished at the EM level by whether the headpiece is closed or open (36). It has been demonstrated using four unique

Fabs to the βI and hybrid domains that stabilizing the closed headpiece of $\alpha_X\beta_2$ inhibits binding to iC3b, whereas stabilizing the open headpiece activates ligand binding (31). Therefore, the effects of mutating or using antibodies to the β-propeller or βI domain must be interpreted with caution, because effects might be indirect by regulating ligand binding by the αI domain.

Exchange of β_2 βI domain residues 177–181 or 203–208 for sequences in the β_1 and β_3 subunits, respectively, decreases $\alpha_M\beta_2$ binding to both fibrinogen and iC3b by about 10-fold (28). These residues abut the specificity-determining loop of the integrin βI domain, and line the pocket that surrounds the βI MIDAS and relays integrin activation from the βI domain to the αI domain by binding α_X residue Glu-318 (29). The above two exchanges thus likely act by disrupting communication between the αI and βI domains. Direct binding of the βI domain to ligands was also suggested, based on binding in an ELISA of an immobilized peptide with βI residues 176–187 to fibrinogen and iC3b and a peptide with βI residues 281–291 to iC3b. However, it is unlikely that the first peptide could assume its structure in a βI domain β-sheet (29) as a peptide, and the second peptide is buried in an interface with the α_X β-propeller domain, and thus is unavailable for ligand binding in its native configuration in $\alpha_X\beta_2$ (29). Furthermore, this second peptide is far from and on the opposite face of the βI domain from the first peptide; thus, the two peptides fail to define a ligand-binding site.

Another study used exchanges between the integrins $\alpha_M\beta_2$ and $\alpha_2\beta_1$ to map ligand binding to the α_M β-propeller domain (27); however, the α_M and α_2 subunits are only 26% identical (38), and marked incompatibilities may thus be introduced by such exchanges. For example, exchange of the α_M I domain into $\alpha_2\beta_1$ failed to yield binding to iC3b, most likely because the α_2 β-propeller domain and β_1 βI domain were unable to activate the α_M αI domain. The same study mapped iC3b binding to the fourth blade of the α_M β-propeller domain (27). All of five exchanges in blade 4 reduced binding by 4- to 60-fold, whereas no exchanges in blades 5, 6, or 7 had effects. The segments exchanged in blade 4 correspond in the $\alpha_X\beta_2$ structure to residues at the "bottom" of the β-propeller in the β1-β2 and β3-β4 loops (residues 394–401 and 417–425), residues at the "top" of the β-propeller in the β1-β4 loop (residues 380–384), residues on the side of the β-propeller in the β4-strand (residues 426–433), and residues buried in the β-propeller in the β3-strand and in the interface with the βI domain (residues 408–416). Because these correspond to all three faces of the β-propeller domain and a buried segment, they cannot define a ligand-binding site. The most likely interpretation is that the β-propeller/βI domain interface that is involved in the βI-αI allostery relay mechanism was disrupted. This interpretation is plausible because the nondisruptive segments exchanged in blades 5, 6, and 7 are all more distal from this interface than the segments in blade 4. Of four synthetic peptides tested, one corresponding to α_X residues 406–422 bound to iC3b. It is difficult to rationalize this result structurally, because most of this peptide is buried as a β-propeller β3-strand and the few exposed residues, near each end of the peptide, are distal from one another structurally.

We have previously found that binding of integrins $\alpha_M\beta_2$ and $\alpha_X\beta_2$ to iC3b could be completely inhibited by antibodies to the α_M or α_X αI domain, respectively (14, 24). Adhesion of $\alpha_M\beta_2$ to iC3b could also be inhibited by antibody CBRM1/32 to the β-propeller domain (24). After deletion of the α_M I domain, some adhesion to iC3b substrates (25% of WT levels) was uncovered. This binding was completely inhibited by mAb CBRM1/32 and EDTA. The CBRM1/32 mouse anti-human epitope is completely abolished by substituting human Arg-534 with its mouse equivalent, Gln (39). The equivalent Arg-531 residue in the $\alpha_X\beta_2$ structure (29) is in the β2-β3 loop of β-propeller blade 6, near the β_2 βI and hybrid domains and far from the β-propeller interface with the βI MIDAS, and even further (90 Å) from the αI MIDAS. Simultaneous binding of iC3b or C3c to the αI domain MIDAS and to the β-propeller near α_X-R531 appears unlikely because the MIDAS and R531 are far from one another and face in opposite directions in the $\alpha_X\beta_2$ ectodomain structure. It remains possible that deletion of the α_M I domain uncovers a binding site for iC3b at the β_2 MIDAS and that the CBRM1/32 mAb inhibits both αI- and βI-dependent adhesion by an allosteric mechanism.

Our EM results demonstrate binding of the αI domain of $\alpha_X\beta_2$ to iC3b and C3c. When the complex is adsorbed to the EM grid and dried, the integrin and iC3b/C3c are forced to lie in the same plane. In solution, the major planes of the integrin headpiece and iC3b/C3c may be closer to perpendicular than parallel, because in occasional class averages, the relative orientations of C3c and $\alpha_X\beta_2$ were reversed, although maintaining exactly the same association site. Notably, in all orientations visualized, the C3c moiety was far from the α_X β-propeller domain and β_2 βI domain. Thus, although we cannot rule out an interaction with these domains that was obscured by flattening on the substrate, our data are most consistent with the interpretation that the β-propeller and βI domains have a regulatory rather than direct role in binding.

Our previous EM study on C3 showed that in iC3b, the TED moiety was attached to the C3c moiety through a flexible linker corresponding to a portion of the CUB domain remaining after release of the C3f fragment by factor I (6). The TED moiety appeared in different positions relative to the C3c moiety in class averages derived from a minority of particles; however, in most class averages, the TED moiety was averaged out. Whereas the TED accounts for 19% of mass in iC3b, the TED accounts for only 6% of mass in the complex with $\alpha_X\beta_2$ and three Fabs. The flexible integrin and the three Fabs, not all of which are seen in all class averages, account for 68% of mass. Therefore, these components of the complexes dominate over the TED in the K-means classification and averaging process, and, as expected, the TED was not seen in class averages. To test this explanation, we used the same EM grids from which our integrin-iC3b-Fab particles were derived and picked particles containing a C3c-like moiety with no associated integrin (particles from which the integrin had dissociated after gel filtration and before or during grid preparation) (Fig. S2*C*). The resulting class averages replicated our previous results (6), with a TED-like moiety appearing in 21 of 50 class averages and the C3c moiety appearing in 43 of 50 class averages (Fig. S2*D*).

Twelve of the class averages on dissociated iC3b in which densities for both the TED and C3c moieties were clear enough to orient them relative to one another (Fig. S2*D*) were further analyzed. All but the C3c moiety was masked, and the class averages were aligned based on the C3c moiety. The class averages were then unmasked (Fig. 3*A*). The TED was most frequently seen on the thick side of the MG ring toward which the C345c knob is cocked. The CUB domain, in which the TED is inserted, is attached (Fig. 3 *B* and *C*, asterisks) to the MG ring between MG7 and MG8. The MG7 and MG8 domains are on opposite sides of the key ring; however, in C3b, the CUB and TED domains are located closer to the thick side of the key ring (Fig. 3*C*). The TED domains resolved in different iC3b class averages are distributed in position (Fig. 3*C*) around the position of the CUB domain in C3b (Fig. 3*B*). We also recalculated the iC3b class averages from our earlier study (6) (Fig. S4). The results show a distribution of TED positions (Fig. S4 *A* and *B*) very similar to that shown in Fig. 3*B*.

A recent EM study on iC3b found a fixed location for the TED and CUB domains near the C345c knob (7). One possible reason for this discrepancy is that Alcorlo et al. (7) did EM on a fraction at the very leading edge of the iC3b peak in gel filtration, whereas Nishida et al. (6) did EM on a fraction at the center of the iC3b peak. The increase in hydrodynamic radius predicted in iC3b by Nishida et al. (6) was confirmed by measuring Stokes radii in gel filtration. The Stokes radius of iC3b was 58.7 Å, whereas those of

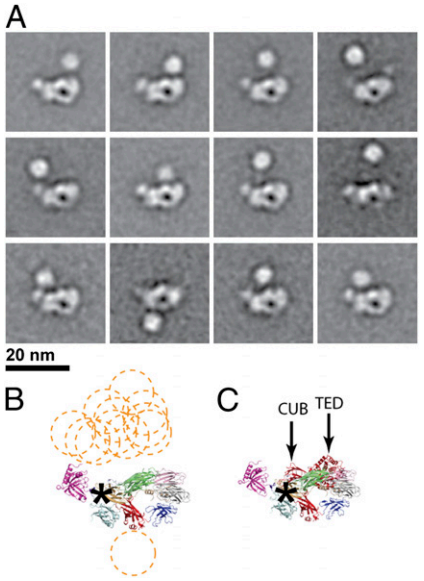

Fig. 3. iC3b class averages and schematics. (*A*) Class averages from particles picked from grids containing iC3b–$\alpha_X\beta_2$–three Fab complexes that appeared to represent dissociated iC3b and were C3c-like in appearance. All 12 of 50 class averages with sufficiently good density for both the TED and C3c moieties to orient them relative to one another are shown. They are aligned based on the C3c moiety. (*B*) Ribbon diagram of C3c (PDB ID code 2A74) in the same orientation as the C3c moiety in *A* (*Top Left*), with the positions of the TED domains in different panels in *A* shown with dashed circles. (*C*) Ribbon diagram of C3b (PDB ID code 2I07), superimposed on and moved horizontally on the page relative to C3c in *B*. Asterisks show the positions of the N- and C-terminal CUB domain residues 912 and 1,330, which are adjacent to one another and link to MG7 and MG8, respectively.

C3, C3(N)*, and C3b were all between 53.4 and 54.7 Å. This showed much greater extension of the CUB and TED domains away from the C3c body in iC3b than in C3, C3(N)*, or C3b. The great contribution of the CUB and TED to the Stokes radius in iC3b was further confirmed in the drop from 58.7 Å in iC3b to 49.5 Å in C3c (6).

Some of the data in Alcorlo et al. (7) were also consistent with these results. Thus, although extra density was seen in class averages in panels 1, 2, and 5 in figure 1B of ref. 7, panels 3 and 4 look similar to our own iC3b class averages. Furthermore, the SAXS data in the study by Alcorlo et al. (7) show a shift to smaller distances in the main distance distribution peak in iC3b compared with C3 and C3b, which is not seen in the iC3b EM model. In contrast, our model of iC3b does predict such a shift (Fig. S5). Furthermore, the large extra blob of density seen near the C345c knob in EM is not seen in the SAXS envelope of iC3b (7). As pointed out by Alcorlo et al. (7), it is possible that there are two interconverting structures for iC3b, one with a random orientation of the TED (6) and another with the TED associated with the C3c moiety (7).

Our EM results show that there is a specific integrin-binding site on iC3b at the interface between the MG3 and MG4 domains. We found no evidence that the TED or CUB domain contributed to binding, because there was no extra density associated with $\alpha_X\beta_2$ corresponding to these domains and there was also no density for them in the position described by Alcorlo et al. (7). Our result with iC3b suggested that the binding site was contained within the C3c moiety. We confirmed this result by preparing complexes with C3c and finding exactly the same binding site at the interface between the MG3 and MG4 domains. These findings significantly advance the long-standing quest to define the integrin-binding site within iC3b (19–21). $\alpha_X\beta_2$ and $\alpha_M\beta_2$ can recognize a wide array of ligands. Furthermore, multiple sites can be recognized within a single ligand. Binding has been implicated to as many as 11–18 sites within denatured or proteolyzed fibrinogen (18). In contrast, the binding to iC3b and C3c appears to be highly specific, because $\alpha_X\beta_2$ was seen to bind only a single, unique site. The region recognized by $\alpha_X\beta_2$ is similarly exposed at the interface between MG3 and MG4 in different C3 fragments (Fig. 4 *A*–*C*), although between C3 and C3b, there is a marked shift in the orientation between these two domains (Fig. 4*D*). The orientation at this interface is the same between C3b and C3c (Fig. 4*D*) and is expected to be the same in iC3b as in C3c (6).

Interestingly, the orientations of C3b and iC3b on opsonic surfaces are distinct (Fig. 4 *E* and *F*). Although the schematic in Fig. 4*F* is based on the model of Nishida et al. (6), the model of Alcorlo et al. (7) also suggests an orientation of iC3b distinct from that of C3b with the region in MG3/MG4 more exposed. The intact CUB domain in C3b orients the TED with respect to the C3c moiety (3, 4). Covalent linkage to the pathogen surface through the TED, as well as a strong electropositive patch on the same face of the TED, is predicted to orient C3b, with its TED, MG1, MG4, and MG5 domains binding to negatively charged surfaces as shown in Fig. 4*E* (4). In contrast, after factor I cleaves in the C-terminal portion of the CUB domain, the N-terminal portion of CUB serves as an ∼50-Å long flexible connection between the surface-attached TED domain and the C3c moiety of iC3b (6) (Fig. 4*F*). In iC3b, the C3c moiety can be presented ∼100 Å further above the surface than in C3b, and in an orientation much better for $\alpha_X\beta_2$ recognition (Fig. 4*F*). Whereas the

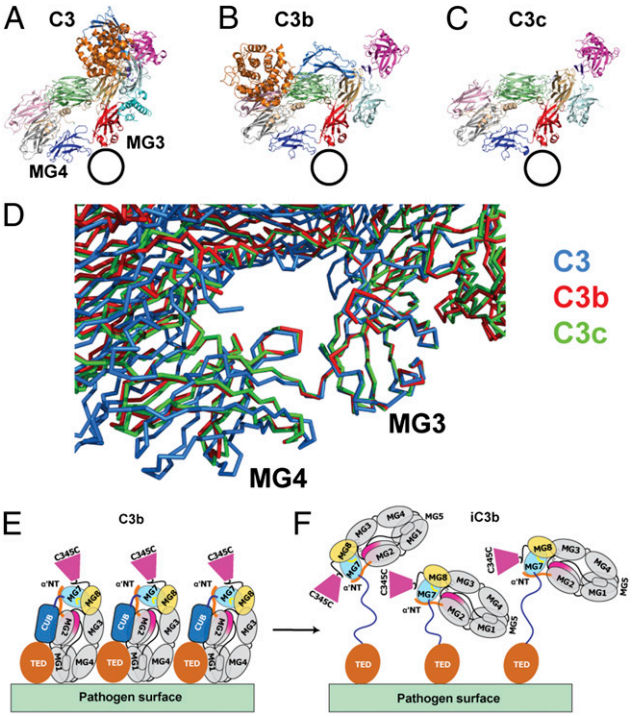

Fig. 4. Crystal structure comparisons and schematics of opsonic surfaces. (*A*–*C*) Ribbon diagrams showing the different positions of the TED and CUB domains in C3 and C3b and their absence in C3c (3–5). Superposition on the key ring shows that the MG3-MG4 interface is exposed in C3, C3b, and C3c; the binding site for the α_X I domain established here with C3c and iC3b is shown as a circle. (*D*) C3, C3b, and C3c superimposed using the MG3 domain. (*E* and *F*) Schematic diagram showing the dense packing and orientations of C3b and iC3b on opsonic surfaces. The arrangement in *E* is based on the C3b binding orientation and density proposed by Janssen et al. (4). The arrangement in *F* is based on *E* and on the flexible connection between the C3c and TED moieties of iC3b (6).

face of the TED contacting the opsonic surface is electropositive, the C3c moiety of iC3b is electronegative (4), and thus would be repelled by biological surfaces, which are generally electronegative. Furthermore, the tether between these two moieties attaches to MG7 at a point on the key ring opposite from MG3 and MG4 (Fig. 4*F*), enabling their optimal exposure on opsonic surfaces. Selectivity of CR4 for iC3b over C3b may be related to the differing orientations of the MG3/MG4 interface in iC3b and C3b on opsonic surfaces.

Materials and Methods

Protein Preparation. Production in CHO Lec 3.2.8.1 cells, purification, treatment with TEV protease, and further purification were as described previously for a soluble $\alpha_X\beta_2$ fragment containing disulfide-linked GCG sequences after the α_X and β_2 ectodomain sequences (29). Human iC3b and C3c were from Complement Technology. The murine mAbs CBR LFA-1/2 (40) and KIM127 (41) have been previously described. m24 (42) was a generous gift from Nancy Hogg (Cancer Research UK London Research Institute, London, UK). IgGs were purified with a protein A column. Fab fragments were prepared with bead-immobilized papain using the Pierce Fab preparation kit (Pierce Chemical Co.).

Negative-Stain EM. The $\alpha_X\beta_2$ ectodomain (13 μg) was incubated with iC3b (60 μg) or C3c (120 μg) in the presence of $\alpha_X\beta_2$ activating Fabs (16 μg each) in a total volume of 60 μL. Complexes were isolated by Superdex 200 chromatography in 20 mM Tris·HCl (pH 7.5), 150 mM NaCl, 2 mM $MnCl_2$, and 0.5 mM $CaCl_2$. Peak fractions were adsorbed to glow-discharged carbon-coated copper grids and stained with uranyl formate, and low-dose images were acquired with an FEI Tecnai-12 transmission electron microscope at 120 kV and a nominal magnification of 67,000× using a defocus of −1.5 μm.

Image processing was performed with SPIDER and EMAN as previously described (31). From 2,000 to 5,000 particles were picked interactively and subjected to multireference alignment and K-means classification specifying 50 or 100 classes. The most populous classes representing the range of conformations and most structural details are shown in the main text.

For cross-correlation, the EM density corresponding to iC3b or C3c was isolated from the class average images by masking out other parts. The crystal structure of C3c (PDB ID code 2A74) (5) was inflated by 10%, Fourier-transformed, filtered to 20 Å with a Butterworth low-pass filter, and transformed back. Evenly spaced projections at intervals of 4° from the crystal structure were subjected to 10 cycles of alignment with masked EM class averages. The cross-correlation coefficient is reported for the most similar crystal structure projection. The EM density for the α_X I domain was similarly isolated and cross-correlated with the α_X I domain crystal structure (PDB ID code 3K71) to determine its precise position in the class averages (17).

ACKNOWLEDGMENTS. We thank A. Koksal for calculations for Fig. S5. This work was supported by National Institutes of Health Grant AI72765. X.C. is a Pfizer Fellow of the Life Sciences Research Foundation. T.W. is an investigator in the Howard Hughes Medical Institute.

1. Walport MJ (2001) Complement. First of two parts. *N Engl J Med* 344:1058–1066.
2. Carroll MC (2004) The complement system in regulation of adaptive immunity. *Nat Immunol* 5:981–986.
3. Wiesmann C, et al. (2006) Structure of C3b in complex with CRIg gives insights into regulation of complement activation. *Nature* 444:217–220.
4. Janssen BJ, Christodoulidou A, McCarthy A, Lambris JD, Gros P (2006) Structure of C3b reveals conformational changes that underlie complement activity. *Nature* 444: 213–216.
5. Janssen BJ, et al. (2005) Structures of complement component C3 provide insights into the function and evolution of immunity. *Nature* 437:505–511.
6. Nishida N, Walz T, Springer TA (2006) Structural transitions of complement component C3 and its activation products. *Proc Natl Acad Sci USA* 103:19737–19742.
7. Alcorlo M, et al. (2011) Unique structure of iC3b resolved at a resolution of 24 Å by 3D-electron microscopy. *Proc Natl Acad Sci USA* 108:13236–13240.
8. Ross GD, Lambris JD (1982) Identification of a C3bi-specific membrane complement receptor that is expressed on lymphocytes, monocytes, neutrophils, and erythrocytes. *J Exp Med* 155:96–110.
9. Yan J, et al. (2000) Critical role of Kupffer cell CR3 (CD11b/CD18) in the clearance of IgM-opsonized erythrocytes or soluble β-glucan. *Immunopharmacology* 46:39–54.
10. Tang T, et al. (1997) A role for Mac-1 (CDIIb/CD18) in immune complex-stimulated neutrophil function in vivo: Mac-1 deficiency abrogates sustained Fcgamma receptor-dependent neutrophil adhesion and complement-dependent proteinuria in acute glomerulonephritis. *J Exp Med* 186:1853–1863.
11. Beller DI, Springer TA, Schreiber RD (1982) Anti-Mac-1 selectively inhibits the mouse and human type three complement receptor. *J Exp Med* 156:1000–1009.
12. Micklem KJ, Sim RB (1985) Isolation of complement-fragment-iC3b-binding proteins by affinity chromatography. The identification of p150,95 as an iC3b-binding protein. *Biochem J* 231:233–236.
13. Malhotra V, Hogg N, Sim RB (1986) Ligand binding by the p150,95 antigen of U937 monocytic cells: Properties in common with complement receptor type 3 (CR3). *Eur J Immunol* 16:1117–1123.
14. Bilsland CAG, Diamond MS, Springer TA (1994) The leukocyte integrin p150,95 (CD11c/CD18) as a receptor for iC3b. Activation by a heterologous β subunit and localization of a ligand recognition site to the I domain. *J Immunol* 152:4582–4589.
15. Davis GE (1992) The Mac-1 and p150,95 β_2 integrins bind denatured proteins to mediate leukocyte cell-substrate adhesion. *Exp Cell Res* 200:242–252.
16. Gahmberg CG, Tolvanen M, Kotovuori P (1997) Leukocyte adhesion—Structure and function of human leukocyte β2-integrins and their cellular ligands. *Eur J Biochem* 245:215–232.
17. Vorup-Jensen T, Ostermeier C, Shimaoka M, Hommel U, Springer TA (2003) Structure and allosteric regulation of the $\alpha_X\beta_2$ integrin I domain. *Proc Natl Acad Sci USA* 100: 1873–1878.
18. Vorup-Jensen T, et al. (2005) Exposure of acidic residues as a danger signal for recognition of fibrinogen and other macromolecules by integrin alphaXbeta2. *Proc Natl Acad Sci USA* 102:1614–1619.
19. Wright SD, Reddy PA, Jong MTC, Erickson BW (1987) C3bi receptor (complement receptor type 3) recognizes a region of complement protein C3 containing the sequence Arg-Gly-Asp. *Proc Natl Acad Sci USA* 84:1965–1968.
20. Taniguchi-Sidle A, Isenman DE (1992) Mutagenesis of the Arg-Gly-Asp triplet in human complement component C3 does not abolish binding of iC3b to the leukocyte integrin complement receptor type III (CR3, CD11b/CD18). *J Biol Chem* 267:635–643.
21. Taniguchi-Sidle A, Isenman DE (1994) Interactions of human complement component C3 with factor B and with complement receptors type 1 (CR1, CD35) and type 3 (CR3, CD11b/CD18) involve an acidic sequence at the N-terminus of C3 α′-chain. *J Immunol* 153:5285–5302.
22. Michishita M, Videm V, Arnaout MA (1993) A novel divalent cation-binding site in the A domain of the β_2 integrin CR3 (CD11b/CD18) is essential for ligand binding. *Cell* 72: 857–867.
23. McGuire SL, Bajt ML (1995) Distinct ligand binding sites in the I domain of integrin $\alpha_M\beta_2$ that differentially affect a divalent cation-dependent conformation. *J Biol Chem* 270:25866–25871.
24. Diamond MS, Garcia-Aguilar J, Bickford JK, Corbi AL, Springer TA (1993) The I domain is a major recognition site on the leukocyte integrin Mac-1 (CD11b/CD18) for four distinct adhesion ligands. *J Cell Biol* 120:1031–1043.
25. Ueda T, Rieu P, Brayer J, Arnaout MA (1994) Identification of the complement iC3b binding site in the β_2 integrin CR3 (CD11b/CD18). *Proc Natl Acad Sci USA* 91: 10680–10684.
26. Yalamanchili P, Lu C, Oxvig C, Springer TA (2000) Folding and function of I-domain deleted Mac-1 and LFA-1. *J Biol Chem* 275:21877–21882.
27. Li Y, Zhang L (2003) The fourth blade within the β-propeller is involved specifically in C3bi recognition by integrin $\alpha_M\beta_2$. *J Biol Chem* 278:34395–34402.
28. Xiong YM, Haas TA, Zhang L (2002) Identification of functional segments within the β2I-domain of integrin alphaMbeta2. *J Biol Chem* 277:46639–46644.
29. Xie C, et al. (2010) Structure of an integrin with an alphaI domain, complement receptor type 4. *EMBO J* 29:666–679.
30. Nishida N, et al. (2006) Activation of leukocyte β_2 integrins by conversion from bent to extended conformations. *Immunity* 25:583–594.
31. Chen X, et al. (2010) Requirement of open headpiece conformation for activation of leukocyte integrin alphaXbeta2. *Proc Natl Acad Sci USA* 107:14727–14732.
32. Emsley J, Knight CG, Farndale RW, Barnes MJ, Liddington RC (2000) Structural basis of collagen recognition by integrin $\alpha_2\beta_1$. *Cell* 101:47–56.
33. Shimaoka M, et al. (2003) Structures of the alpha L I domain and its complex with ICAM-1 reveal a shape-shifting pathway for integrin regulation. *Cell* 112:99–111.
34. Song G, et al. (2005) An atomic resolution view of ICAM recognition in a complex between the binding domains of ICAM-3 and integrin alphaLbeta2. *Proc Natl Acad Sci USA* 102:3366–3371.
35. Luo B-H, Carman CV, Springer TA (2007) Structural basis of integrin regulation and signaling. *Annu Rev Immunol* 25:619–647.
36. Springer TA, Dustin ML (2012) Integrin inside-out signaling and the immunological synapse. *Curr Opin Cell Biol* 24:107–115.
37. Goodman TG, Bajt ML (1996) Identifying the putative metal ion-dependent adhesion site in the β2 (CD18) subunit required for alphaLbeta2 and alphaMbeta2 ligand interactions. *J Biol Chem* 271:23729–23736.
38. Yu Y, et al. (2012) Structural specializations of $\alpha_4\beta_7$, an integrin that mediates rolling adhesion. *J Cell Biol* 196:131–146.
39. Lu C, Oxvig C, Springer TA (1998) The structure of the β-propeller domain and C-terminal region of the integrin alphaM subunit. *J Biol Chem* 273:15138–15147.
40. Petruzzelli L, Maduzia L, Springer TA (1995) Activation of LFA-1 (CD11a/CD18) and Mac-1 (CD11b/CD18) mimicked by an antibody directed against CD18. *J Immunol* 155: 854–866.
41. Robinson MK, et al. (1992) Antibody against the Leu-CAM β-chain (CD18) promotes both LFA-1- and CR3-dependent adhesion events. *J Immunol* 148:1080–1085.
42. Dransfield I, Hogg N (1989) Regulated expression of Mg^{2+} binding epitope on leukocyte integrin α subunits. *EMBO J* 8:3759–3765.

Supplemental Information for

Molecular basis for complement recognition by integrin $\alpha_X\beta_2$

Xing Chen[1,2], Yamei Yu[1], Lizhi Mi[1], Thomas Walz[3], and Timothy A. Springer[1,*]

[1] Immune Disease Institute, Children's Hospital Boston and Department of Biological Chemistry and Molecular Pharmacology, Harvard Medical School, Boston, Massachusetts 02115, USA.

[2] Current address: College of Chemistry and Molecular Engineering, Peking University, Beijing, 100871, P.R. China

[3] Howard Hughes Medical Institute and Department of Cell Biology, Harvard Medical School, 240 Longwood Avenue, Boston, Massachusetts 02115, USA.

* Corresponding: Springer@idi.harvard.edu

Fig. S1. The complete set of class averages of $\alpha_X\beta_2$ in complex with CBR LFA-1/2 and KIM127 Fabs. Averages are ranked (left to right in each row, from top to bottom row) by numbers of particles in each class.

Fig. S2. The $\alpha_X\beta_2$-3 Fabs-iC3b complex and iC3b alone. (A) Representative EM image. (B) The complete set of class averages after picking complex-like particles. (C) Another representative EM image, with particles boxed that are C3c-like and have dissociated from the integrin. (D) The complete set of class averages resulting from picking dissociated, C3c-like particles Averages are ranked (left to right in each row, from top to bottom row) by numbers of particles in each class.

Fig. S3. The $\alpha_X\beta_2$-3 Fabs-C3c complex. (A) Representative EM image. (B) The complete set of class averages. Averages are ranked (left to right in each row, from top to bottom row) by numbers of particles in each class.

Figure S4. Comparison of data of Alcorlo et al. to SAXS calculated from crystal structures. (A and B) Previously published results (7). (A) Plots are the distribution of distances within proteins derived from SAXS measurements on C3, C3b, or iC3b or calculated from the Alcorlo et al. iC3b EM structure. Note that the main peak is shifted to the left for the iC3b protein preparation but not for the model iC3b (EM). (B) Protein envelopes calculated from SAXS (7). Note that the iC3b SAXS envelope lacks the extra density near the C345c knob found in EM by (7). (C) Protein distance distributions calculated from crystal structures for C3 (PDB ID code 2A73 (5)), C3b (PDB ID code 2I07 (4)), C3c (PDB ID code 2A74 (5)), and from 3 models of iC3b. Models of iC3b were made by removing the C3f fragment (residues 1281-1298) from the C3b structure, and rotating a segment containing residues 951-1280 (the TED plus two CUB β-strands) about an origin centered on residues 950 and 951. SAXS data were calculated for three models with the TED swung at different angles away from C3c moiety. P(r) distributions for the three models were averaged and shown in panel C. (D) Figure 4 from (7). The iC3b model is from EM and the C3 and C3b models are from crystal structures filtered to a similar resolution. Note that while the models from SAXS data in (B) reproduce reasonably the shapes of C3 and C3b, there is less correspondence between the iC3b SAXS model in (B) and the EM model in (D). The SAXS model of iC3b looks not unlike the structure of C3c.

The most robust result from the SAXS data of (7) is the position of the main P(r) peak in (A), since scattering at long distances given by C3, C3b, or iC3b in (A) at > 150 Å is influenced by aggregates and is not seen in distance distributions calculated from the EM data in (A) or from crystal structures in (C). In the experimental data of Alcorlo et al. (A), the main P(r) peak of iC3b shifts to smaller distances compared to C3 and C3b, reflecting a loss of mass from the

main center of mass in iC3b; which may correspond to movement away of the TED moiety from the C3c moiety. In P(r) distributions calculated from crystal structures the main peak in the P(r) distributions calculated from the iC3b model in (C) shows a similar shift to the left compared to C3 and C3b as seen for iC3b protein but not the iC3b (EM) model in (A). However, the SAXS data calculated from the iC3b models in (C) is shifted more to the right than the experimental iC3b data in (A). Thus, the TED may swing away a lesser amount than in the models, or may equilibrate to a position in contact with the C3c moiety as suggested by Arcorlo et al.

Figure S5. Recalculation of class averages for iC3b. The same particles as previously picked (6) were used to recalculate class averages, choosing 100 rather than 200 classes. (A) All particles showing a TED moiety and C3c moiety were aligned on the C3c moiety. (B) A cartoon diagram of C3c, aligned on the class average in the upper left panel in (A), is shown in the same orientation, with the position of the TED moiety in all class averages shown in A marked as broken circles. (C) A cartoon diagram of C3b, superimposed on C3c in (B), and separated horizontally on the page. Both (B) and (C) are enlarged relative to class averages in (A). (D) The complete set of 100 class averages. Averages are ranked (left to right in each row, from top to bottom row) by numbers of particles in each class.

$\alpha_x\beta_2$ + CBR LFA-1/2 and KIM 127
(4,502 particles, 50 classes)
Particles in the extended, open headpiece conformation: >95%

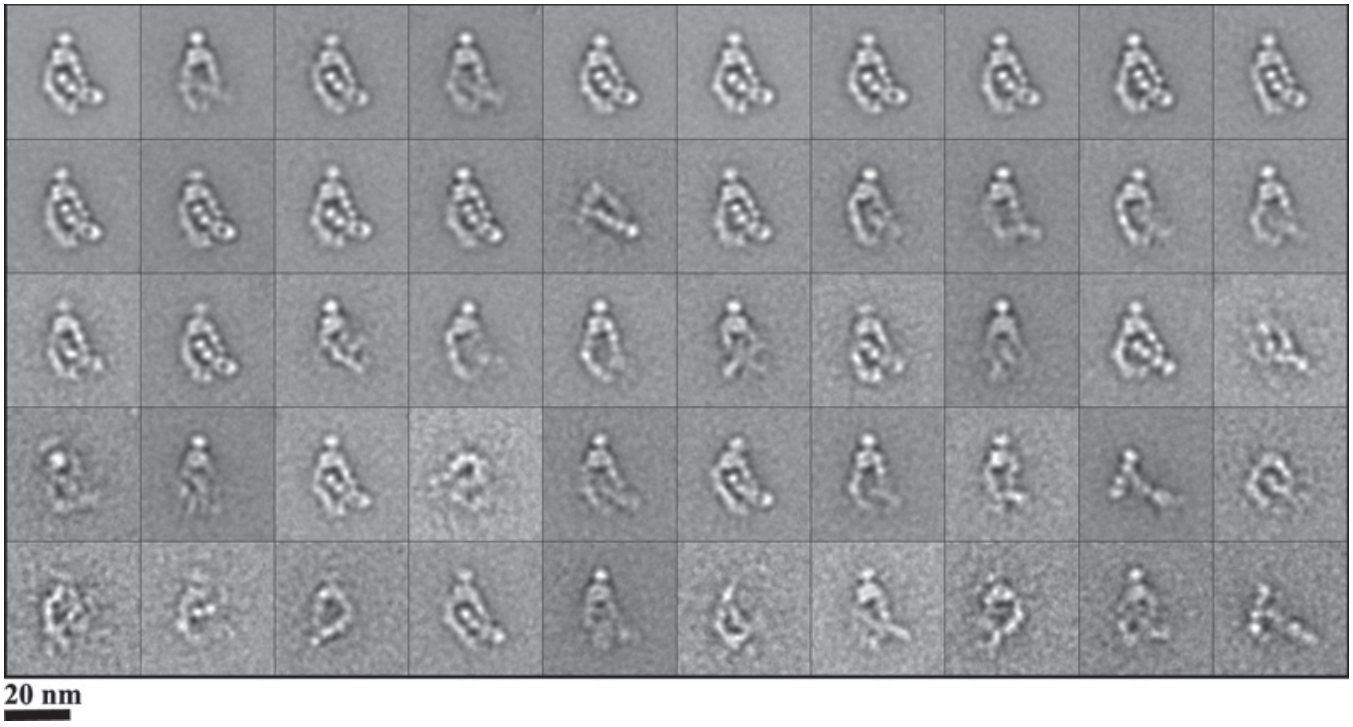

Figure S1.

A

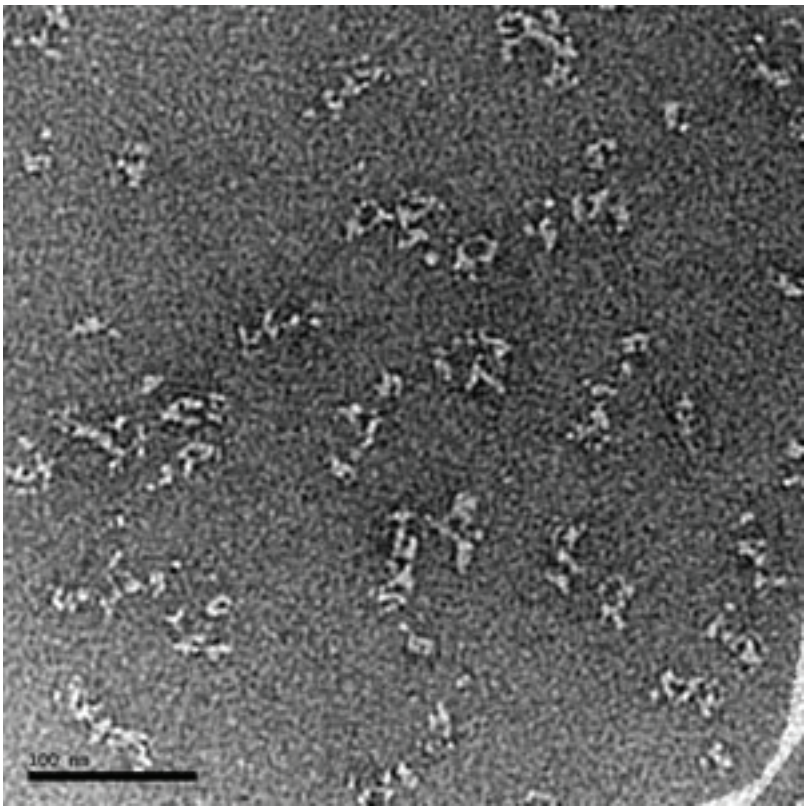

B $\alpha_x\beta_2$ + CBR LFA-1/2, KIM 127, and m24 + iC3b (5,134 particles, 50 classes)

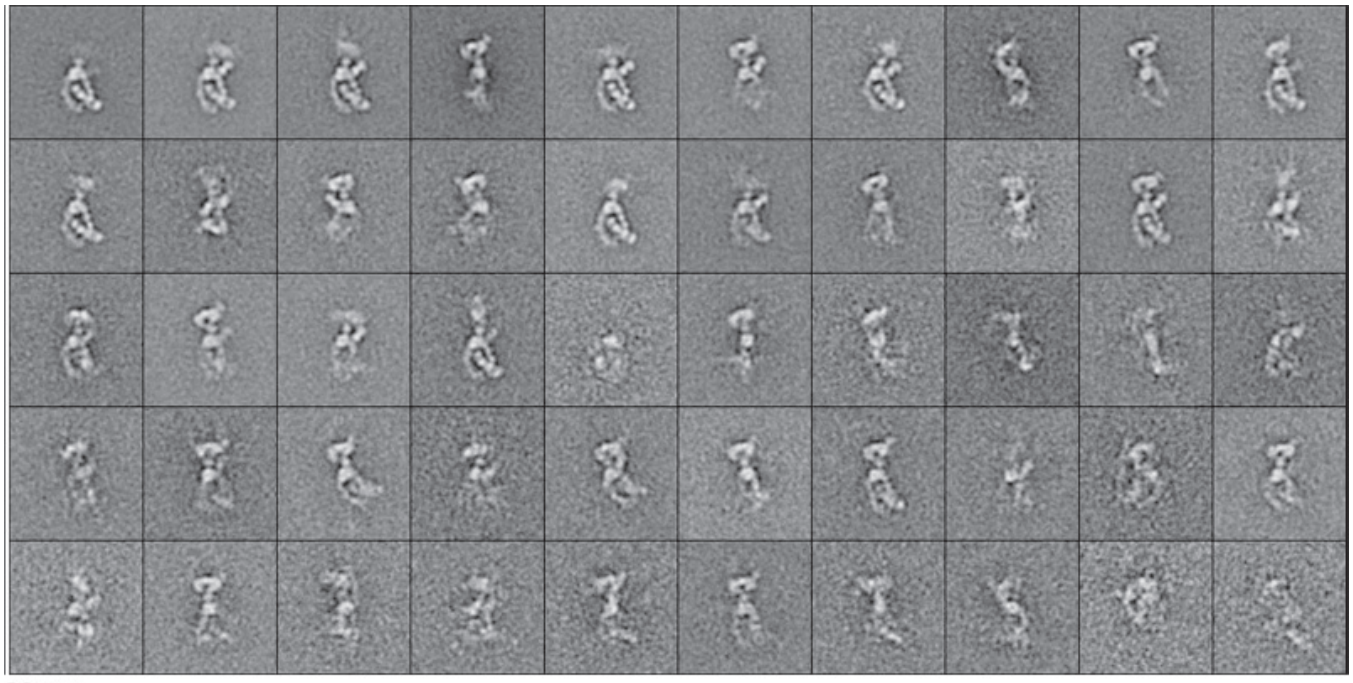

Figure S2A,B

C

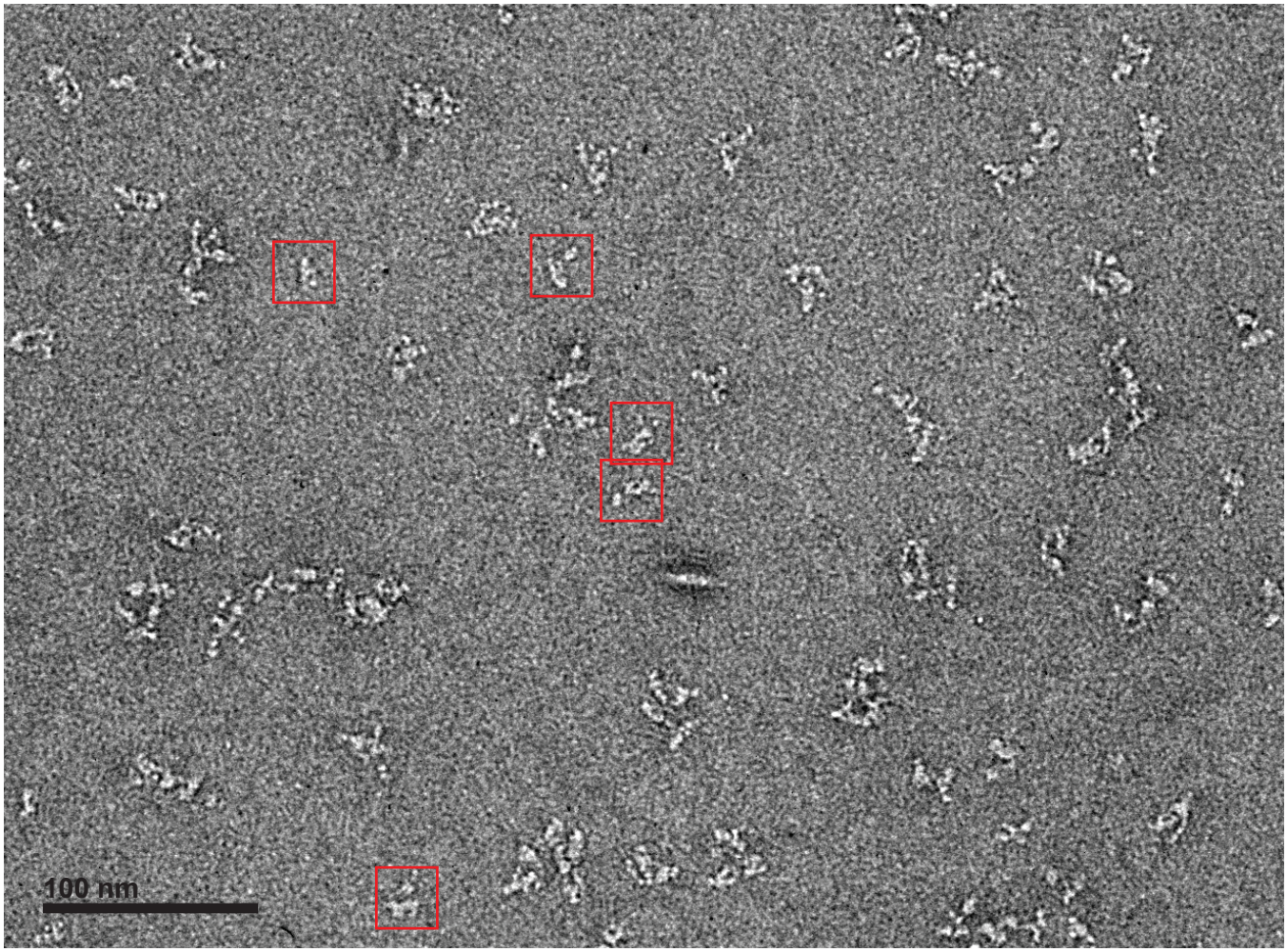

D $\alpha_X\beta_2$ + CBR LFA-1/2, KIM 127, and m24 + iC3b (2,487 C3-like particles picked, 50 classes)

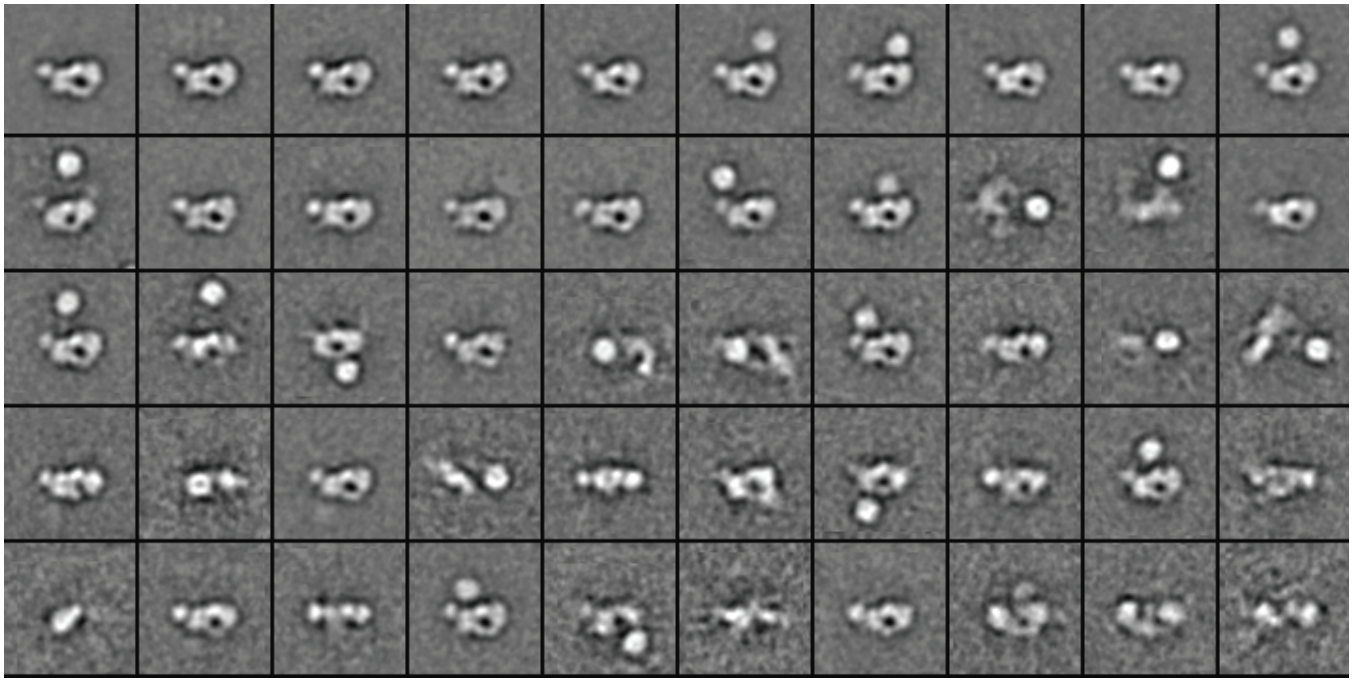

20 nm

Figure S2C,D

A

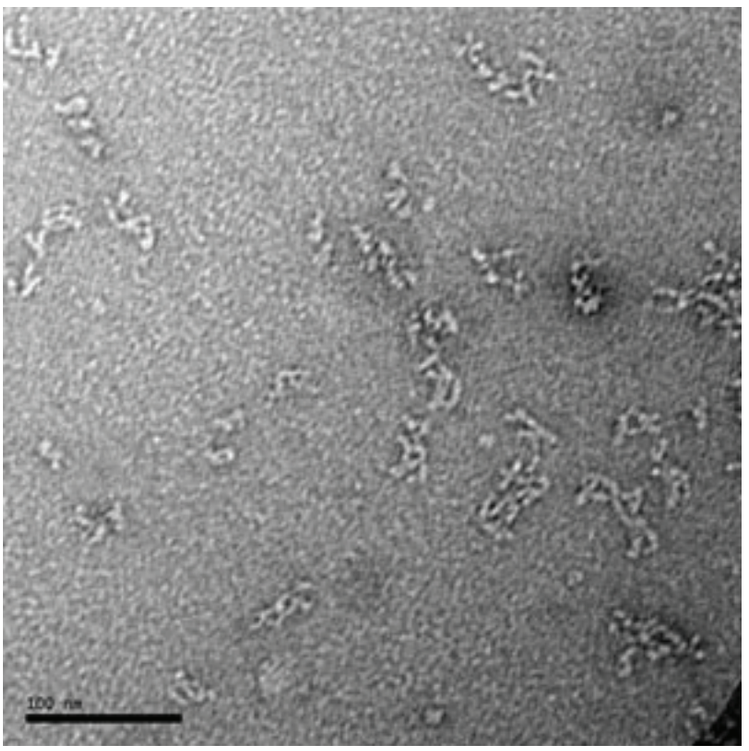

B

$\alpha_x\beta_2$ + CBR LFA-1/2, KIM 127, and m24 + C3c (4,387 particles, 100 classes)

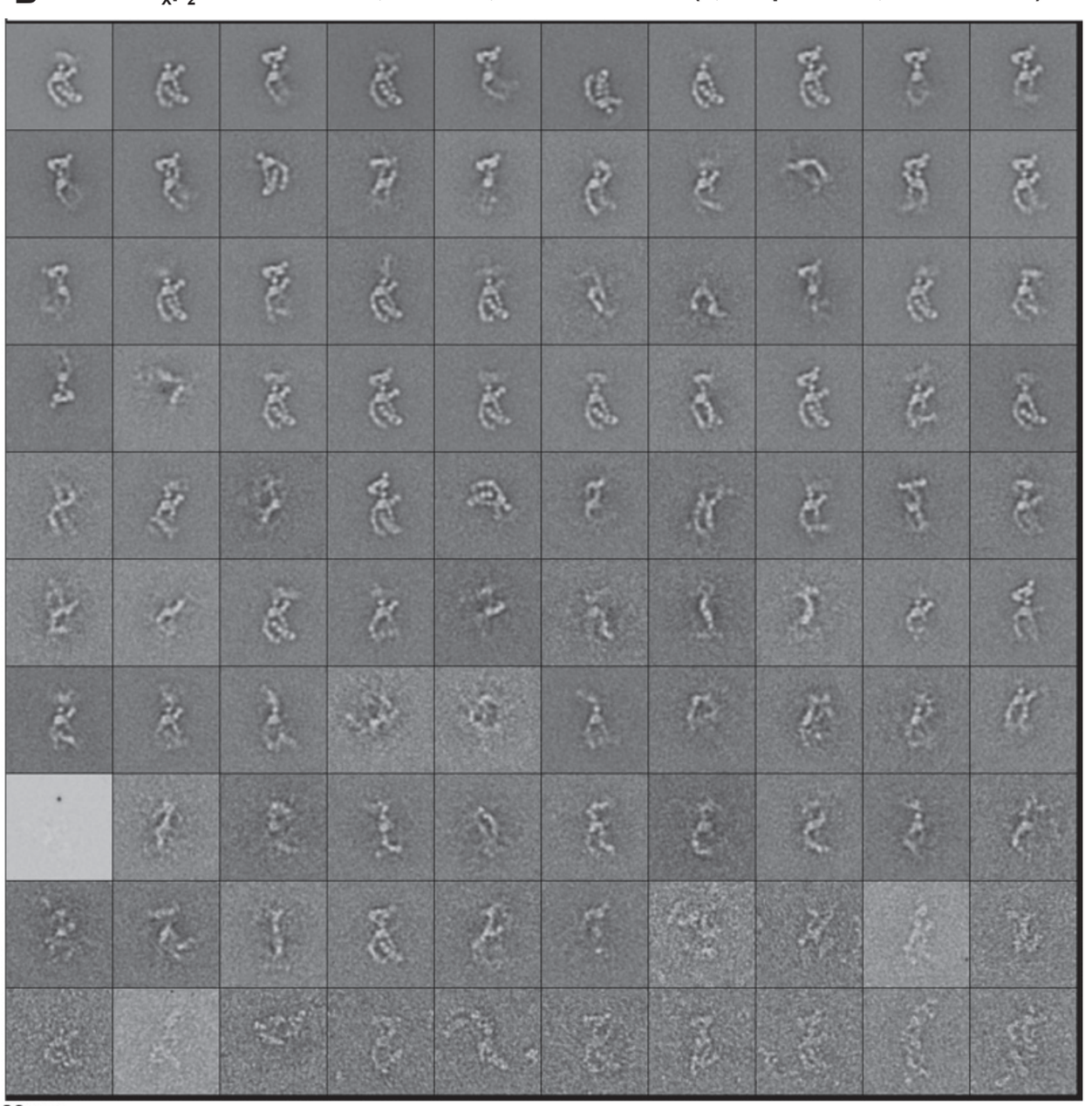

Figure S3

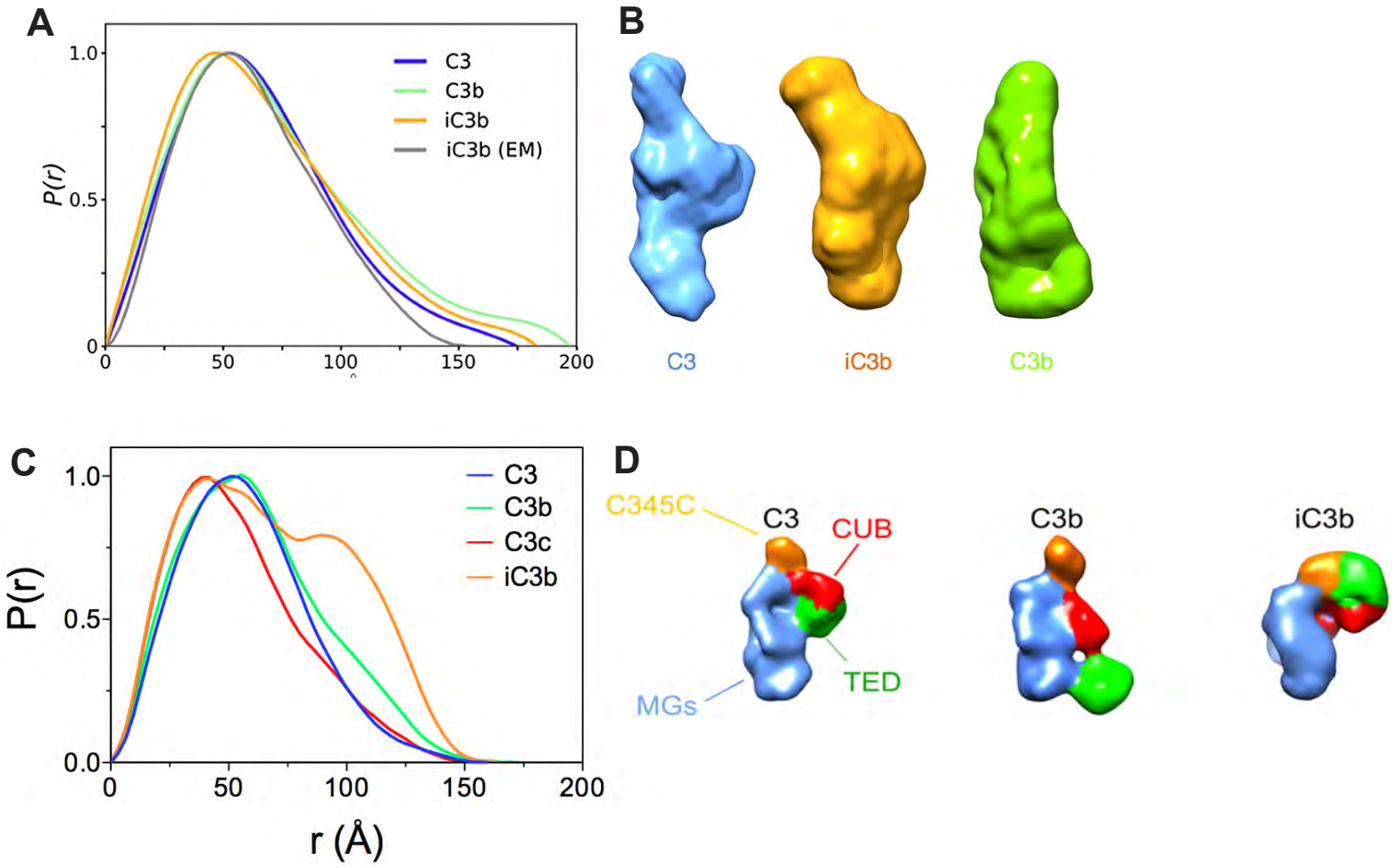
A
1.0
0.5
0
P(r)
0
50
100
150
200
C3
C3b
iC3b
iC3b (EM)
B
C3
iC3b
C3b
C
1.0
0.5
0.0
P(r)
0
50
100
150
200
r (Å)
C3
C3b
C3c
iC3b
D
C345C
C3
CUB
TED
MGs
C3b
iC3b

Figure S4

A

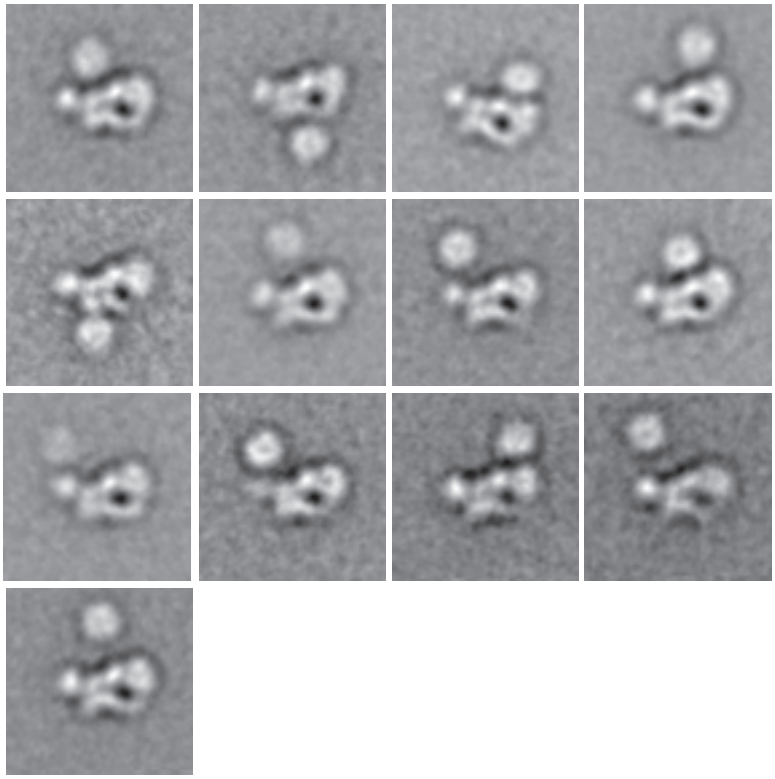

20 nm

B

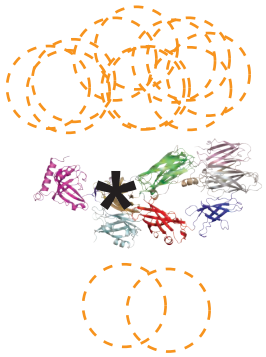

C

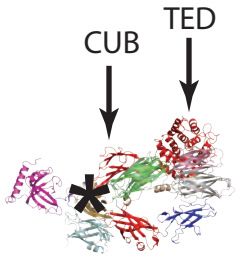

Figure S5A,B,C

D **iC3b (5,445 particles picked, 100 classes)**

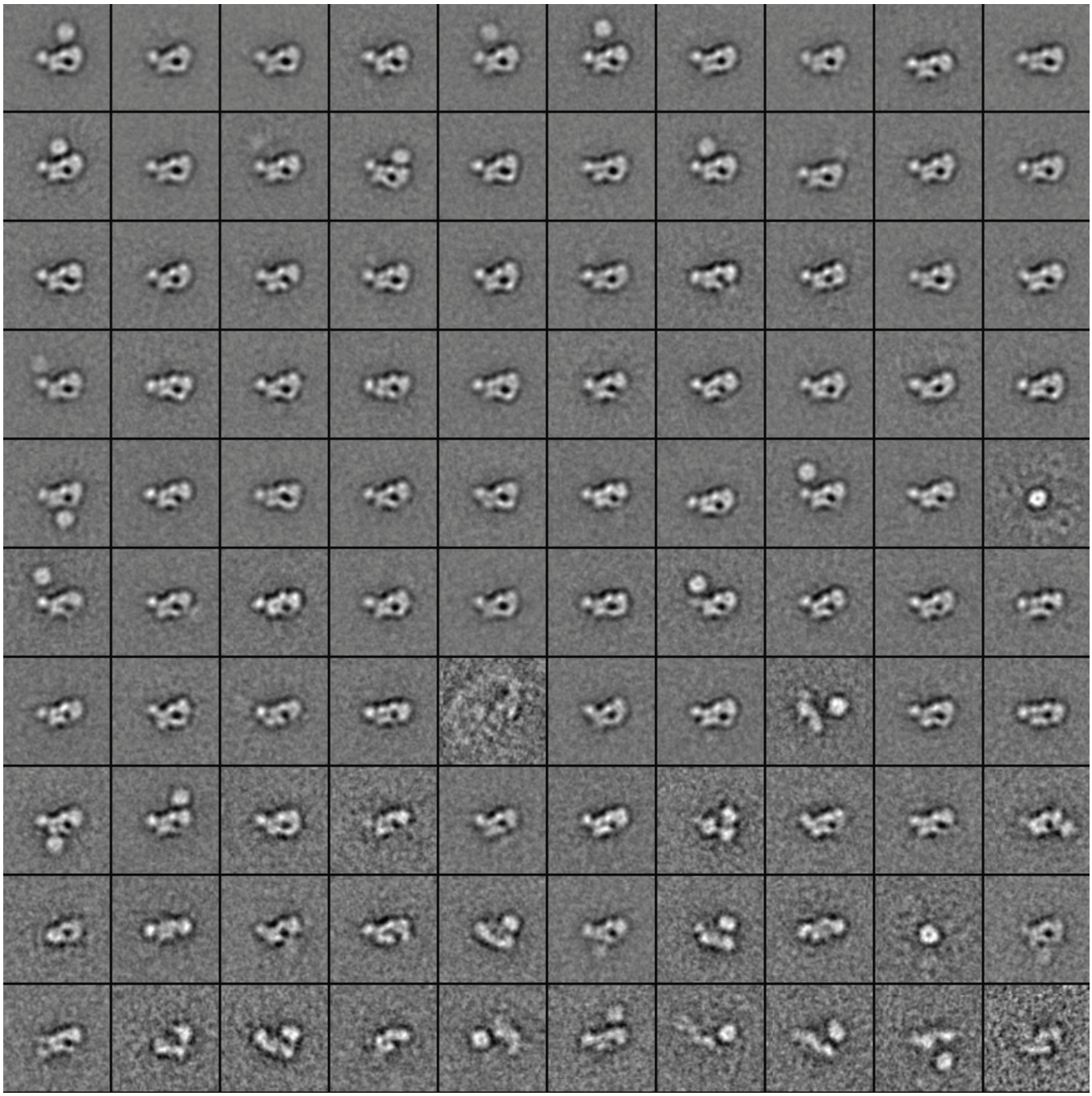

20 nm

Figure S5D